Chapter 3

Event selection

In this chapter the b-quark event selection is described. We started with the events that satisfy the "electron" requirement in the CDF trigger system during the run time. However, substantial amount of the non-electron background still remains in this stage. We apply tighter electron identification criteria to remove the non-electron background events. Additional requirements on the remaining events are made to enrich the b-quark event fraction. It also ensure the good measurements of some variables (Impact parameter, p_T^{rel}) used to estimate the b-quark event fraction. Finally the diffractive candidates are selected from the b-quark candidates by the rapidity gap tagging.

3.1 $b\bar{b}$ candidate selection

3.1.1 Central electron trigger

We start from the data sets which includes electron candidates observed in the CEM. In this data sets, the following selection criteria have been applied at the level-3 trigger. The terms used in this lists are described later.

- E_T(ele)[1] >7.5 GeV
- P_T(ele)>6.0 GeV/c

[1]The transverse energy is calculated using the nominal interaction point

- L_{SHR} <0.2
- HAD/EM<0.125
- cluster-track matching at the CES: $r\Delta\phi < 3.0$ cm
- cluster-track matching at the CES: $\Delta z < 5.0$ cm
- χ^2_{strip} <10

In order to avoid the trigger bias which kill the rapidity gap events, we ensure that the events are not collected by the level-1 trigger of the west and east BBC coincidence. We selected the events taken by the central electron triggers (CEM_8_CFT_7_5_V* or CEM_8_CFT_7_5_XCES*) in order to compare the physics results to the Monte Carlo simulation which models this trigger.

3.1.2 Electron identification

We first define the electron energy cluster in the central EM calorimeter. Since the lateral size of electromagnetic shower is smaller than the size of single tower, the maximum size of the electron cluster is restricted to the 3 towers in the η direction and only one tower in the ϕ direction $[0.3(\eta)\times15°(\phi)]$. The E_T threshold used for the clustering is 0.1 GeV. The "electron track" is defined as the highest momentum track which points to the electron energy cluster.

Electron identification at the CDF is basically performed using a signature of electromagnetic shower development in the EM calorimeter and the presence of the track in the CTC.

However, a charged hadron which leaves a track in the CTC can mimic the electron signature in the calorimeter by the energy deposition through the π^0s production in the material. The produced π^0 immediately decays into two photons that start an electromagnetic shower. This background

("hadron faking electron") is difficult to separate since the shower shape is basically identical to the electron.

Another source of event which mimics the electron signature is an overlap hit of a charged hadron and photons on the same calorimeter cluster. In the Tevatron, most of photons are produced by $\pi^0 \rightarrow \gamma\gamma$ decays in the QCD jet. Those two photons from the π^0 decay tend to point to the single electron energy cluster since the two photon system is highly boosted toward the calorimeter comparing to the pion mass. The lateral shape of such electromagnetic shower caused by two photons is different from the single electron's one and this property is used to reject those events.

In order to suppress the above non-electron backgrounds we applied the following electron identification cuts:

Hadronic energy fraction: HAD/EM

A ratio of hadronic to electromagnetic cluster energy HAD/EM is used to identify the isolated electromagnetic shower signature. We use the upper bound of the HAD/EM of 0.04 when a single CTC track is pointing to the calorimeter energy cluster. When multiple tracks are pointing to the cluster, we loosen the upper bound of the HAD/EM to 0.10.

Energy momentum ratio: E/p

The energy and momentum match is required since we selected isolated energy cluster for an electron candidate. This cut is useful to reject the accidental overlap of charged hadrons and photons. We used the allowable E/p range from 0.75 to 1.4.

Lateral shower shape adjacent towers: L_{SHR}

The energy sharing in adjacent towers for electrons is very different from that for an overlap of photon and hadron. Most electrons deposit the energy on a

single CEM tower since the typical lateral size of electromagnetic shower is smaller than the tower size. On the other hand, an overlap event of charged hadron and multiple photons could leave extra energies in towers adjacent to a seed tower by multi-photon hit. So this type of background can be suppressed by requiring a tower energy profile in a three-tower sum cluster.

The lateral shower profile L_{SHR} [29] is defined by comparing the measured energy sharing to the test beam data.

$$L_{SHR} = 0.14 \times \sum_i \frac{E_i^{adj} - E_i^{prob}}{\sqrt{0.14^2 E + (\Delta E_i^{prob})^2}}.$$

Here, E_i^{adj} is the measured energy in the tower adjacent to the seed tower; E_i^{prob} is the expected energy in that tower calculated from the seed energy of the cluster, the impact point from the strip chamber, and the event vertex using a shower profile parameterization from test beam data; E is the EM energy in the cluster; and ΔE_i^{prob} is the error in E_i^{prob} associated with a 1-cm error in the impact point measurement. The sum is over the two towers adjacent to the seed tower in the same azimuthal wedge. We required L_{shr} to be less than 0.2 for an electron candidate.

Lateral shower shape in a seed tower: CES χ^2

A finer profile of a lateral shower shape in the seed tower is measured using strip and wire information of the CES. This profile is also used to reject the overlapping background.

In the CES, 11 strips (18~23cm) around the peak channel is used to sample the shower shape perpendicular to the beam line. The shower shape along the beam line is also sampled by the CES wires in the same way.

The measured energy distribution in strip and wire channels are compared with those of test beam data to calculate a χ^2. We require the χ^2 to be less than 10.0 for electron candidates in both strip and wire views.

Position matching: $r\Delta\phi, \Delta z \sin\theta$

The position matching of the shower centroid and the electron trajectory is required to reject the overlapping background. The shower centroid of the electron candidate is obtained by fitting the measured lateral profile with the CES to that expected from the test beam profile, as described in the previous section. The position in the local CES coordinate system is represent with (X_{ces},Z_{ces}), corresponding to $r \times \phi$ and z in the CDF coordinate system. The CTC track of the electron candidates is extrapolated to the detector radius where the CES is placed to calculate the deviation of this extrapolated track from the shower centroid. We require the deviation in the r-ϕ view $\Delta X_{ces}(= r\Delta\phi)$ to be less than 1.4 cm. We also require the deviation in the polar angle view $\Delta Z_{ces} \sin\theta (= \Delta z \sin\theta)$ to be less than 2.0 cm.

CPR charge

The CPR charge deposition is useful to reject the hadron faking electrons. Since a hadron hardly start a shower before the CPR layer, it deposits less charge in the CPR than real electrons.

The charge deposition in three CPR wires (6.6 cm) around an 'electron' trajectory are summed and then corrected depending on both the angle and the momentum of the track (see Appendix B).

The CPR charge distribution for real electrons is significantly different from for the hadron rich sample. We used an lower bound of the CPR charge of 2.0 for electron identification, where the selection efficiency for real electron(hadron) is 93%(46%).

3.1.3 Additional requirements

There are several other processes to produce real electrons aside from the b-hadron decay.

One of the main source of the electron is a photon conversion process in the detector material ($\gamma N \rightarrow e^+e^-N$). The Dalitz $\pi^0 \rightarrow e^+e^-\gamma$ decay also produces the real electron. Those events are characterized by the pair production of the two oppositely charged particles (e^+e^-).

The weak boson decay ($W \rightarrow e\nu, Z \rightarrow e^+e^-$) is another source of the real electron. The electron from this process is characterized by a large transverse momentum because of a large mass of the weak boson, ~ 80 GeV/c^2.

The most difficult source of the electron to separate is a semi-leptonic decay of a charm quark. In order to achieve the separation of b-hadron from c-hadron decay, we require a good reconstructed track for the electron in the SVX and an associating jet around the electron track.

The additional requirements for the b-quark candidate selection is described here. Some fundamental quality cuts to ensure the good measurements of the electron energy are also listed.

Photon conversion rejection

The opening angle between the electron-positron pair produced by the photon conversion process is very small since the mass of the parent particle is zero. This is also the case with the electron-positron pair which is produced through a Dalitz decay $\pi^0 \rightarrow e^+e^-\gamma$ because the mass of the parent is much smaller than its kinetic energy.

To identify those events, a conversion partner track of the electron candidate is searched from all CTC tracks ("conversion finding method"). The following cut are applied to an oppositely charged track to the electron candidate:

- $|\delta S| < 0.2$(cm)
- $|\delta \cot\theta| < 0.06$

The $|\delta S|$ is a distance between two trajectories when they become parallel in the r-ϕ plane. The $|\delta \cot\theta|$ represents a parallelism of two trajectories in the r-z plane defined by the difference between $\cot\theta$ of two trajectories. If there exists a track which satisfys the above requirements, we reject the candidate as a conversion electron.

The another method to identify a conversion electron is to look a continuity of the drift chamber tracks. When a photon conversion take place in the material between the two chambers, an ionization track is observed in the outer chamber but not in the inner chamber. We use the hit occupancy of the VTX (VTX_{occ}) to reject the conversions occurring outside the VTX. The VTX_{occ} is defined as a ratio of the number of VTX wire hits to the number of wires which are expected to be fired by a particle.

- $VTX_{occ} > 0$

Ideally, we should not have such "outside" conversions in the sample because we require a hit in the SVX placed inside the VTX. However, it is possible to link the hits in the SVX to the wrong CTC track in the actual track reconstruction.

Weak boson rejection

W decay events ($W \rightarrow e\nu$) is characterized by a large missing E_T and a large electron E_T. The missing E_T, denoted by $\not\!\!E_T$ is defined to be the vector sum of transverse energy in calorimeter towers over the pseudorapidity range $|\eta|$ <3.6;

$$\not\!\!E_T = \left| -\sum_{|\eta|<3.6} \overrightarrow{E_T} \right| .$$

We use the following cuts to reject W decays:

- E_T(ele) < 20GeV

- $\not\!\!E_T < 20$GeV

The electron from $Z \rightarrow e^+e^-$ decay also has a large E_T. This event is also rejected by the above electron E_T cut.

electron E_T

We require the electron to have an E_T above 9.5 GeV in order to minimize a bias on the E_T spectrum due to a trigger inefficiency. The trigger efficiency depends on both E_T and P_T.

- E_T(ele) > 9.5GeV

Track quality

For the high precision measurement of the impact parameter, we require the electron to have a good reconstructed track in the SVX. We require the track to have the hits in at least three SVX layers. The χ^2 of the reconstructed track divided by the number of hit SVX layers is required to be less than 6.

- $N_{svx} \geq 3$
- $\chi^2_{svx}/N_{svx} < 6$

In the CTC, reconstructed electron track was required to have at least 2 axial layers with at least 5 hits each and at least 2 stereo layers with at least 2 hits each.

Vertex position

To ensure the good energy measurement in the projected tower geometry of the calorimeter, we require z_0 of the electron track to be within 60 cm of the nominal interaction point. However, this cut is somewhat too deliberate because we require the electron to have a hit in the SVX which is ±26 long in z direction.

- $|z_0$(ele)$| < 60$cm

Associating jet requirement

In order to measure the p_T^{rel} (see Sec. 5.2), the associating jet is required for the electron track. Jets are reconstructed by clustering tracks in the CTC, using the following algorithm [30]: all 'good' tracks with $p_T > 1.0$ GeV/c are found and placed into an array of 'seed' tracks; the seed tracks are looped over and if another seed track lies within the cone R=0.4, where $R^2 = \Delta\eta^2 + \Delta\phi^2$, then the two seeds are merged into one by summing their momenta vectorally; this process is iterated until no new merging occur; the final phase of clustering consists of merging 'good' tracks with $p_T > 0.4$ GeV/c that lie within the seed cones. Once the jets have been clustered, p_T^{rel} is calculated using the jet that is closest to the electron in R.

In this clustering algorithm, the 'good' track is defined by the following conditions: the good track is reconstructed as a 3D track; the track have at least 2 axial layers with at least 5 hits each and at least 2 stereo layers with at least 2 hits each; the track has a common origin to the electron track, $|z_0 - z_0(\mathrm{ele})| < 5$cm; the impact parameter of the track is within 5.0 cm.

The associating jet to the electron is required to have at least 3 tracks including the electron track.

Summary of the selection criteria

All selection criteria listed above are summarized in Table 3.1. We obtain 161,775 electron candidates using the above selection criteria.

3.2 Diffractive candidate selection: Rapidity gap tagging

The diffractive b-quark production events in the about 160k electron candidates are extracted using a rapidity gap method [10, 11].

We used two kinds of forward detectors in the rapidity gap analysis: the

$9.5 < E_T(\text{ele}) < 20.0$ GeV
HAD/EM< 0.04 for 1 track
HAD/EM< 0.10 for multiple tracks
$0.75 < E/p < 1.4$
$L_{SHR} < 0.2$
$\chi^2_{strip} < 10.0$
$\chi^2_{wire} < 10.0$
$\Delta X_{ces} < 1.4$ (cm)
$\Delta Z_{ces} sin\theta < 2.0$(cm)
Good fiducial hit in the tower
CPR charge > 2.0
Conversion rejection
$\not\!\!E_T < 20$ GeV
Good SVX track: $N_{svx} \geq 3, \chi^2/N_{svx} < 6$
Good CTC track
Associating jet must be reconstructed for the electron track
$\lvert z_0(\text{ele})\rvert < 60cm$

Table 3.1: Summary of the event selection cuts.

BBC ($5.9 > |\eta| > 3.2$) and the forward calorimeter ($4.2 > |\eta| > 2.4$). The analysis is based on the BBC multiplicity and the number of calorimeter clusters with energy above 1.5 GeV, in the same rapidity side. The cluster energy threshold of 1.5 GeV is used to suppress the calorimeter noise. We make the tower clusters as follows: We pick up the towers with E_T above 0.1 GeV. For the towers with E_T below 0.1 GeV, we apply the additional requirements of E(EM) >0.5 GeV and E(HAD)>0.8 GeV. After this cut, all survived towers neighboring to each other are clustered within the cone size of $\sqrt{(\Delta\eta)^2 + (\Delta\phi)^2}$=0.25.

The correlation plot of the BBC multiplicity N_{BBC} and the cluster multiplicity N_C is shown in Fig. 3.1. The $+\eta$ and $-\eta$ sides are plotted in the same figure. The distinct peak at the zero multiplicity bin ($N_{BBC} = N_C = 0$) is observed in this plot. This is a rapidity gap signature of single diffractive events. This gap is caused by an exchange of colorless object between two incoming beam particles. We define the diffractive signal region to this zero

multiplicity bin. In this diffractive signal region, 100 events are observed. Figure 3.2(a) shows the electron E_T spectrum for the diffractive candidates compared that for the whole electron sample. Those two spectra do not show any significant difference. Figure 3.2(b) shows the pseudorapidity distribution of the electrons. Diffractive candidates tagged with positive rapidity side are plotted after changing the sign of the electron η so that rapidity gap is always come to left side of the plot. The diffractive candidates show a small shift toward the opposite side of the rapidity gap.

The background fit of the non-diffractive events in the signal region is performed using the one-dimensional multiplicity plot (Fig. 3.1(b)) obtained by picking up the diagonal bins in Fig. 3.1(a). We fit the high multiplicity region using a straight line and then extrapolate it to the diffractive signal region. The background fit yields 24.4±5.5 non-diffractive events in the diffractive signal region.

We have checked a possible difference between two rapidity sides. The number of diffractive candidates in each rapidity side is analyzed individually as shown in Fig. 3.3 and Fig. 3.4. The number of diffractive candidates is 38.1±7.7 in the $+\eta$ side and 37.9±8.4 events in the $-\eta$ side. We thus conclude that the difference between two forward detectors is negligibly small.

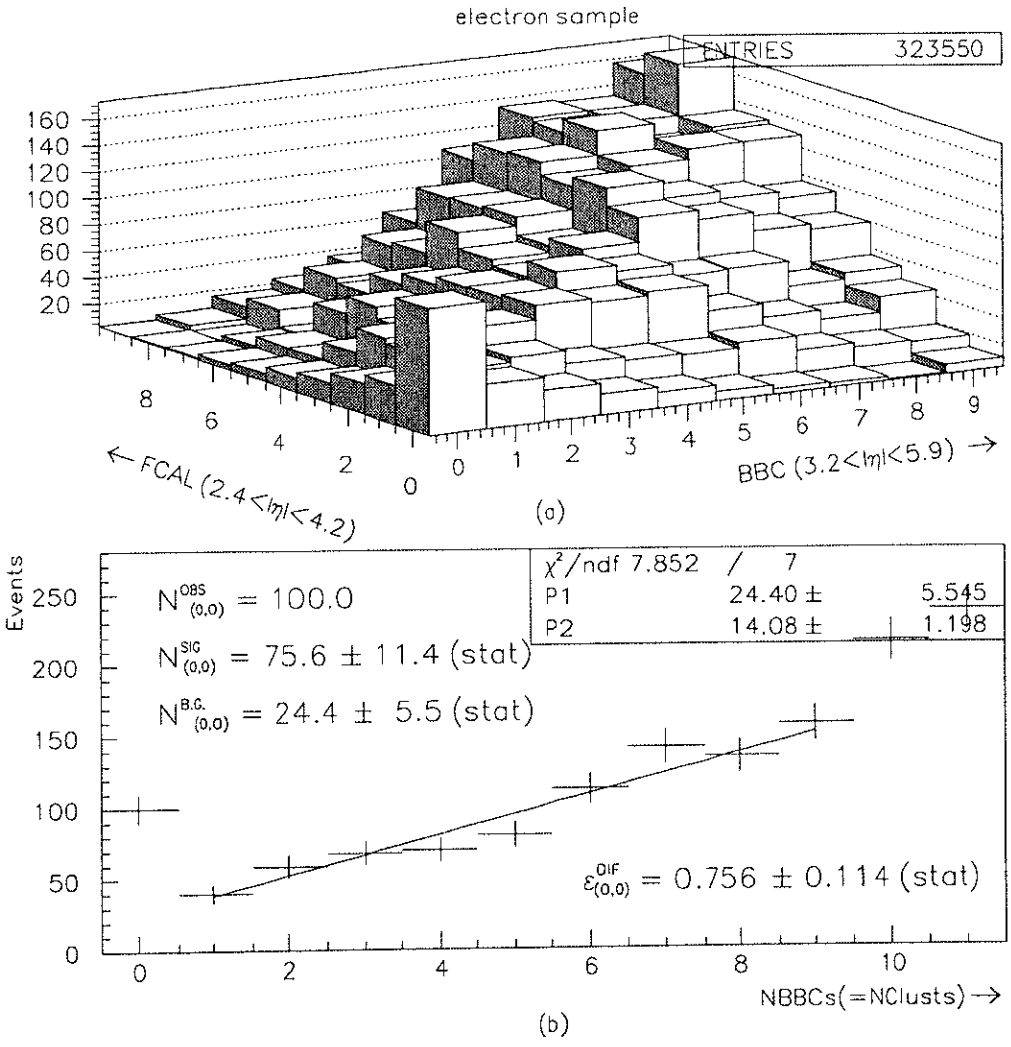

Figure 3.1: (a) BBC multiplicity versus adjacent forward calorimeter cluster multiplicity (two entries per events). (b) Multiplicity along the diagonal axis in the above plot. Non-diffractive background in the zero multiplicity bin is estimated by a streight line fit.

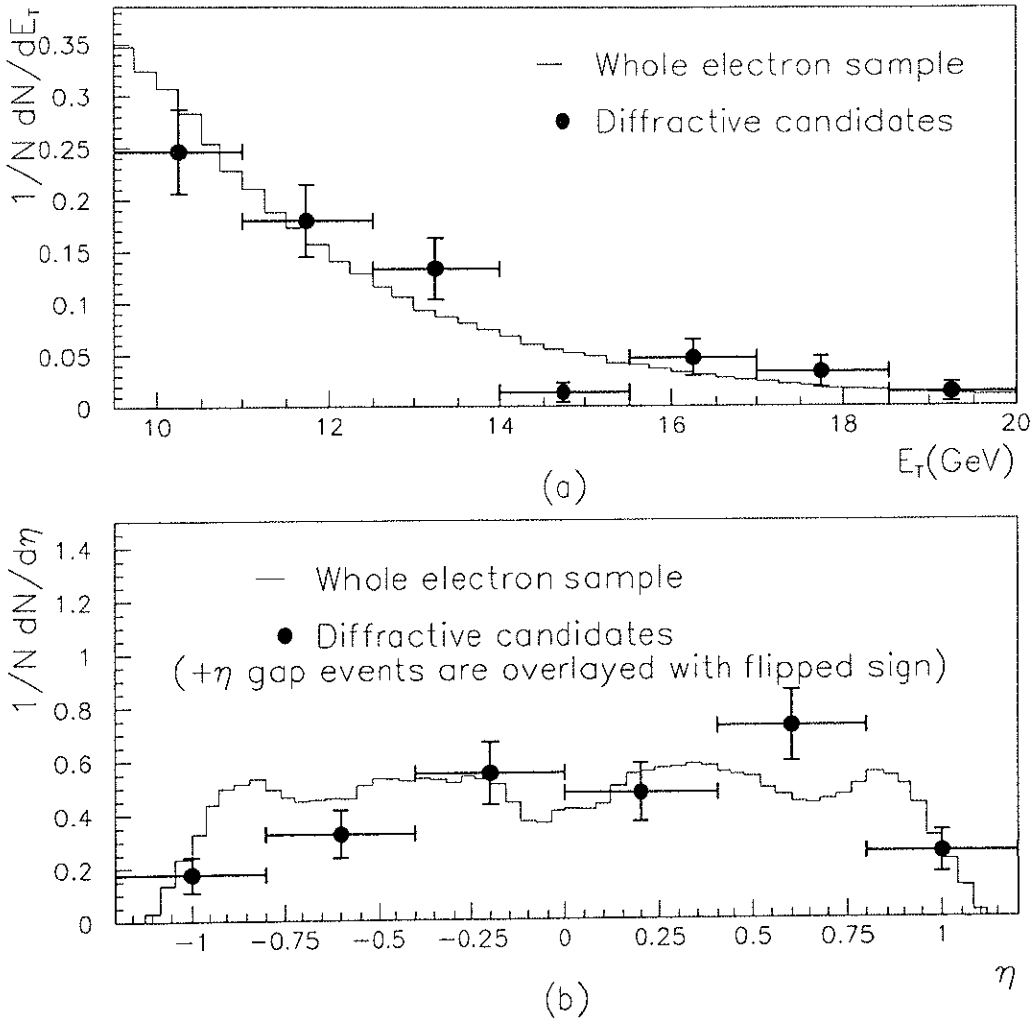

Figure 3.2: (a) Transverse energy spectrum of electrons. The solid histogram shows whole electron sample and solid circles show the diffractive candidates. (b) Pseudorapidity distribution of electrons. The solid histogram shows whole electron sample and black circles show the diffractive candidates. The diffractive candidates tagged by the $+\eta$ side gap are plotted with an inverted sign of its electron pseudorapidity.

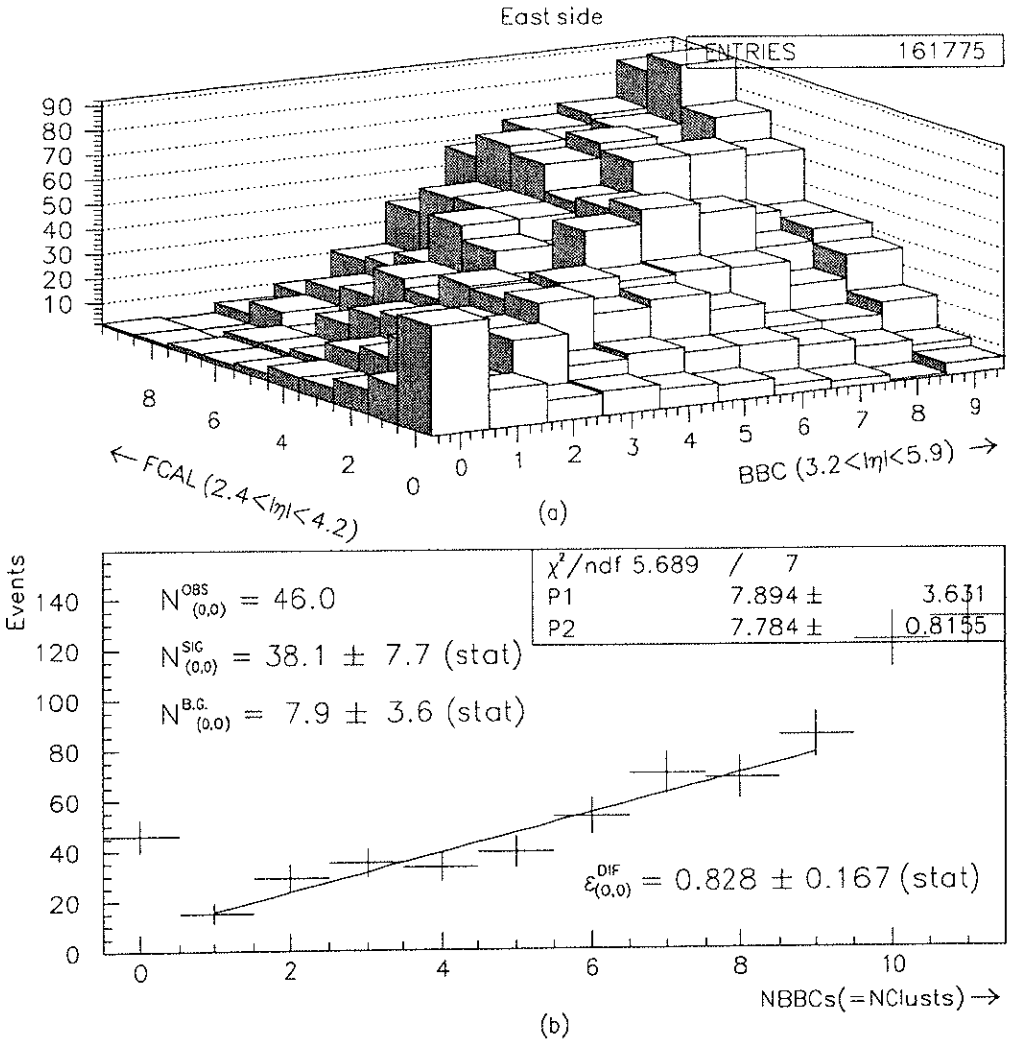

Figure 3.3: (a) BBC multiplicity versus cluster multiplicity in $+\eta$ side (two entries per events). (b) Multiplicity along the diagonal axis in the above plot.

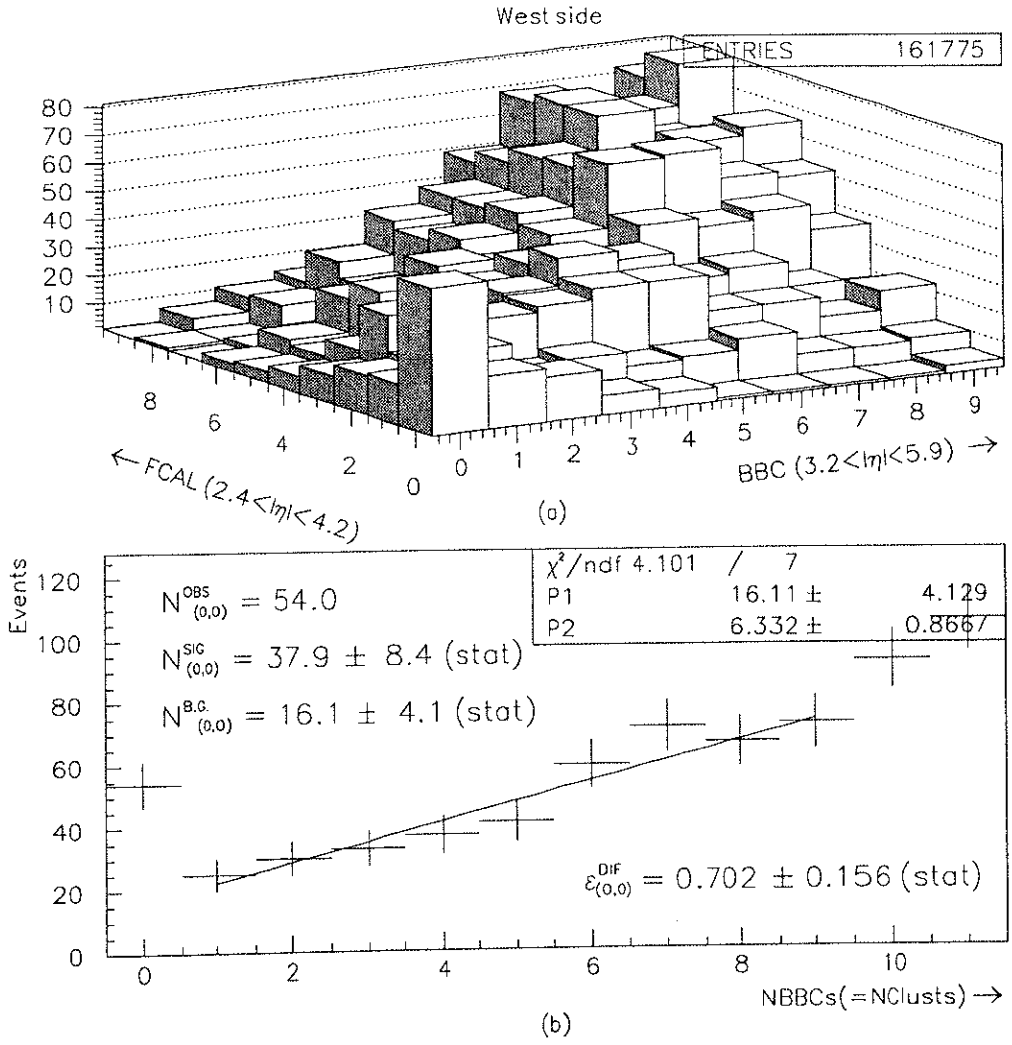

Figure 3.4: (a) BBC multiplicity versus cluster multiplicity in -η side (two entries per events). (b) Multiplicity along the diagonal axis in the above plot.